

Determination of the local structure of the $\text{La}_{0.5-x}\text{Na}_{0.5+x}\text{Fe}_2\text{As}_2$ superconductorG. M. Pugliese,¹ L. Simonelli,² L. Tortora,¹ G. Tomassucci,¹ A. Iyo,³ H. Eisaki,³ T. Mizokawa,⁴ and N. L. Saini^{1,*}¹*Department of Physics, Sapienza University of Rome, P. le Aldo Moro 2, 00185 Roma, Italy*²*CELLS—ALBA Synchrotron Radiation Facility, Carrer de la Llum 2-26, 08290, Cerdanyola del Valles, Barcelona, Spain*³*National Institute of Advanced Industrial Science and Technology (AIST), Tsukuba, Ibaraki 305-8568, Japan*⁴*Department of Applied Physics, Waseda University, Tokyo 169-8555, Japan* (Received 25 June 2021; revised 8 December 2021; accepted 6 January 2022; published 24 January 2022)

We have studied the local structure of $\text{La}_{0.5-x}\text{Na}_{0.5+x}\text{Fe}_2\text{As}_2$ superconductor by As K -edge x-ray absorption fine structure measurements as a function of temperature in a wide range of hole doping ($x = 0.0$ to 0.35). A substantial change in the local structure around the arsenic atom has been observed with doping. The axial As-As_{*a*} bond length is found to be $>\sim 3.12$ Å, indicating that the system is in its collapsed tetragonal phase. The temperature-dependent mean square relative displacements reveal that the As-Fe bond is relatively weak in the undoped sample; however, it gets stronger with hole doping. On the other hand, the axial As-As_{*a*} bond tends to get weaker in the optimally doped regime ($x = 0.25$ – 0.35), suggesting the possible role of increased As atom displacements in the axial direction in the superconducting phase of these materials. Consistently, the arsenic height from the Fe-Fe plane shows a gradual increase in the optimally doped regime. Apart from providing a quantitative information on the local structure of $\text{La}_{0.5-x}\text{Na}_{0.5+x}\text{Fe}_2\text{As}_2$, the results suggest a vital role of electron-lattice coupling and axial As atom displacements in the superconductivity of these iron-based materials.

DOI: [10.1103/PhysRevB.105.024519](https://doi.org/10.1103/PhysRevB.105.024519)**I. INTRODUCTION**

The discovery of superconductivity in the iron pnictides [1] has opened frontiers in the fundamental science and ways to design layered functional materials. Indeed, the discovery has been instrumental in developing a large number of iron-based superconductors characterized by a variety of different structures and physical properties [2–4]. Among iron pnictides, the most known structures are the so-called 1111 (ReFeAsO , where Re stands for rare-earth elements), 122 (AeFe_2As_2 , where Ae stands for alkaline earth, i.e., Ca, Sr, or Ba), and recently grown 1144 ($\text{AeAFe}_4\text{As}_4$, with A being an alkaline atom, i.e., Na or K) [5]. The highest superconducting transition temperature (T_c) $>\sim 50$ K has been found in the electron-doped 1111 system, realized through a partial substitution in the ReO block layers [2–4]. On the other hand, the 122 system has been grown with both electron and hole doping, the latter being more suitable in which Ae^{2+} is substituted by A^+ , while the earlier suffers a substitutional disorder in the FeAs active layer (e.g., substitution of Fe by Co). The 1144 is a hybrid system with an ordered stacking of two different 122 structures, i.e., AeFe_2As_2 and AFe_2As_2 , with the stability of the 1144 structure depending on the size difference between the Ae and A ions [6,7]. The 1144 system shows self-doped superconductivity with a maximum T_c of ~ 36 K [5,6].

Recently, a 122-type pnictide with a chemical formula of $\text{La}_{0.5-x}\text{Na}_{0.5+x}\text{Fe}_2\text{As}_2$ has been synthesized [8,9]. In this system, electron and hole doping can be controlled by changing a relative concentration of La and Na in the block layer without making any direct alteration/substitution in the electronically

active FeAs layer. Indeed, Fe is expected to be in the Fe^{2+} state for the parent compound ($x = 0$), like the undoped 122 structures, and control over the substitution of La^{3+} by Na^+ permits us to manipulate the charge density in the FeAs layer by a single parameter. Therefore, $\text{La}_{0.5-x}\text{Na}_{0.5+x}\text{Fe}_2\text{As}_2$ has been considered a highly suitable system to explore the electron-hole asymmetry without any direct alteration of the FeAs layer [8–11]. The maximum T_c of this system has been found to be ~ 27 K by hole doping [8,9]. The parent compound shows antiferromagnetic order at low temperature, while the normal state properties of both electron- and hole-doped $\text{La}_{0.5-x}\text{Na}_{0.5+x}\text{Fe}_2\text{As}_2$ are argued to be driven by spin fluctuations [12].

Apart from the above, there are several features of this 122 structure. These peculiar features are indicated by a series of studies, e.g., heavily electron-doped LaFe_2As_2 (i.e., $x = -0.5$) exists in two different crystallographic phases; the as-grown sample exhibits a shorter crystallographic c parameter than the same sample annealed [13]. These are so-called collapsed-tetragonal (CT) and uncollapsed-tetragonal (UT) phases of the 122 system [14,15]. The UT phase of LaFe_2As_2 exhibits superconductivity at ~ 12.1 K, while the CT phase is non-superconducting [13]. This recalls the classical case of the CT phase in CaFe_2As_2 showing filamentary superconductivity [16] with the important role of the axial As-As bonding [17–19]. It is also known that the iron magnetic moment gets suppressed in the CT phase [20], and it remains debated if the magnetism drives the collapse or the As-As dimerization is the cause of the suppressed magnetism [17–21]. The Fermi surface of LaFe_2As_2 is different with the well-known hole pockets near the zone center missing [13]. It has been argued that the hole Fermi surface is there but hidden; that can be

* naurang.saini@roma1.infn.it

seen by artificial removal of La $5d$ orbitals in the theoretical calculations [22].

On the other hand, it is known that electronic states near the Fermi surface in the iron-based superconductors are highly sensitive to the atomic displacements [3,23–25]. This aspect has been widely studied by different experimental techniques focusing on the local structure. The superconductivity and magnetism are found to be coupled to the local structure parameters [23–25]. Indeed, the local structure measurements have provided direct information on the magneto-elastic interactions in these materials [26,27]. In addition, superconductivity has been introduced with a $T_c \sim 10$ K in an undoped 122 system by superlattice engineering in which the As-Fe-As angle is optimized to the one in a regular tetrahedron [28]. It should be recalled that the local structure does have a direct role in the electronic nematicity, i.e., controlling the Fe 3 $d_{xz,yz}$ orbitals at the Fermi surface due to broken Fe-Fe lattice symmetry [29]. The nematic fluctuations are believed to enhance the superconductivity in these materials. Furthermore, the nematicity in the iron-based superconductors has been found to have short-range character [30]. For example, hole-doped (Sr,Na)Fe₂As₂ shows orthorhombic fluctuations as a function of doping, with the coherence length of these fluctuations ranging between 1 and 3 nm [30,31]. Recently, a mesoscopic nematic wave has also been observed in the 122 system [32], further underlining the importance of the local structure. Therefore, quantitative information on the local structure of La_{0.5-x}Na_{0.5+x}Fe₂As₂ is expected to be an important ingredient to address the physics of these materials. In La_{0.5-x}Na_{0.5+x}Fe₂As₂, the relative change of La/Na concentration induces variation in the chemical pressure and hence the local atomic displacements that may have some intimate relationship with the superconductivity of the system.

Here, in light of the above, we have studied the local structure of La_{0.5-x}Na_{0.5+x}Fe₂As₂ ($x = 0, 0.1, 0.15, 0.2, 0.25, 0.3, \text{ and } 0.35$) by extended x-ray absorption fine structure (EXAFS) measurements as a function of temperature. EXAFS enables us to obtain the quantitative local structure surrounding the selected atom in the system, and in this paper, we have chosen arsenic as the central atom. The results reveal a systematic evolution of local bond characteristics as a function of doping with a significant effect on the axial As-As_{*a*} bond length that is found to be consistent with a partial CT phase. While the covalent As-Fe bond gets stronger with increasing doping, the axial As-As_{*a*} bond suffers a substantial weakening with a concomitant increase in the arsenic height in the optimally doped superconducting regime. The results suggest the possible role of axial displacements of As atoms in the superconducting phase.

II. EXPERIMENTAL DETAILS

X-ray absorption measurements were performed on a series of well-characterized polycrystalline samples of La_{0.5-x}Na_{0.5+x}Fe₂As₂ ($x = 0, 0.1, 0.15, 0.2, 0.25, 0.3, \text{ and } 0.35$) prepared by the solid-state reaction method. The details on the sample preparation, characterization, and their structural, electrical, and magnetic transport can be found elsewhere [8]. Temperature-dependent As K -edge ($\sim 11\,867$ eV) x-ray absorption measurements were performed

in the transmission mode at the CLAES beamline [33] of the 3 GeV ALBA synchrotron in Cerdanyola del Valles (Barcelona). The synchrotron radiation emitted by a multipole wiggler source was monochromatized by a Si(311) double-crystal monochromator. The samples were finely powdered and mixed uniformly in an organic matrix (cellulose) before pressing into pellets of 7 mm diameter, with their thickness optimized for the As K -edge x-ray absorption jump close to unity. The pellets of the samples were all mounted on the same sample holder attached to the cold finger of a continuous flow liquid nitrogen cooled cryostat, and the temperature was maintained constant within ± 1 K during each measurement. A standard x-ray absorption setup with three ionization chambers mounted in series was used to measure the energy-dependent absorption coefficient of the samples and a reference sample. Three to four absorption scans were acquired at each temperature to ensure the spectral reproducibility and high signal-to-noise ratio.

III. RESULTS AND DISCUSSIONS

The x-ray absorption spectra were measured at seven different temperatures in the range of 80–300 K on seven different samples covering the hole-doped part of the phase diagram of La_{0.5-x}Na_{0.5+x}Fe₂As₂ [8]. A standard procedure using the method based on polynomial spline function fit to the pre-edge subtracted spectra was used to extract the EXAFS oscillations [34,35]. Examples of the EXAFS oscillations extracted from the x-ray absorption spectra for several samples are shown at selected temperatures in Fig. 1 as a function of wave vector (\mathbf{k}). The oscillations are multiplied by k^3 to enhance the high k region. This is to make sure there is an acceptable EXAFS signal at high k values. The signal is clearly visible above the noise level also at higher temperature. There are some evident changes in the EXAFS oscillations apart from the thermal damping, indicating evolution of the local structure with doping and temperature. Some of these changes can be easily recognized in the real space atomic distribution provided by Fourier transform (FT) of the EXAFS oscillations.

The FT magnitudes of the EXAFS oscillations at different temperatures for the selected samples are displayed in Fig. 2. The FTs of the k^3 -weighted EXAFS are performed in the k range of 2.5–17.5 \AA^{-1} using a Gaussian window. The same scale has been used to display the FT magnitudes of different samples. The FTs represent the partial atomic function around the As atom in the La_{0.5-x}Na_{0.5+x}Fe₂As₂ structure. The structure unit cell, shown in Fig. 2 as an inset of the upper panel, contains four Fe atoms as nearest neighbors of arsenic, and their contribution appears as the main peak in the FT magnitudes. The contributions of the next-nearest neighbors La/Na and the axial As appear mixed, producing a minimum and a weak peak structure in the FTs. This is followed by the contribution of four in-plane As atoms (mixed with the contribution of four As atoms in the next layer), appearing as a peak structure in the FTs at ~ 3.50 \AA . The farther atom contributions are mixed with multiple scatterings appearing beyond ~ 3.5 \AA . Apart from a systematic thermal damping, the effect of hole doping on the local structure around the As atom is evident from an overall damping of

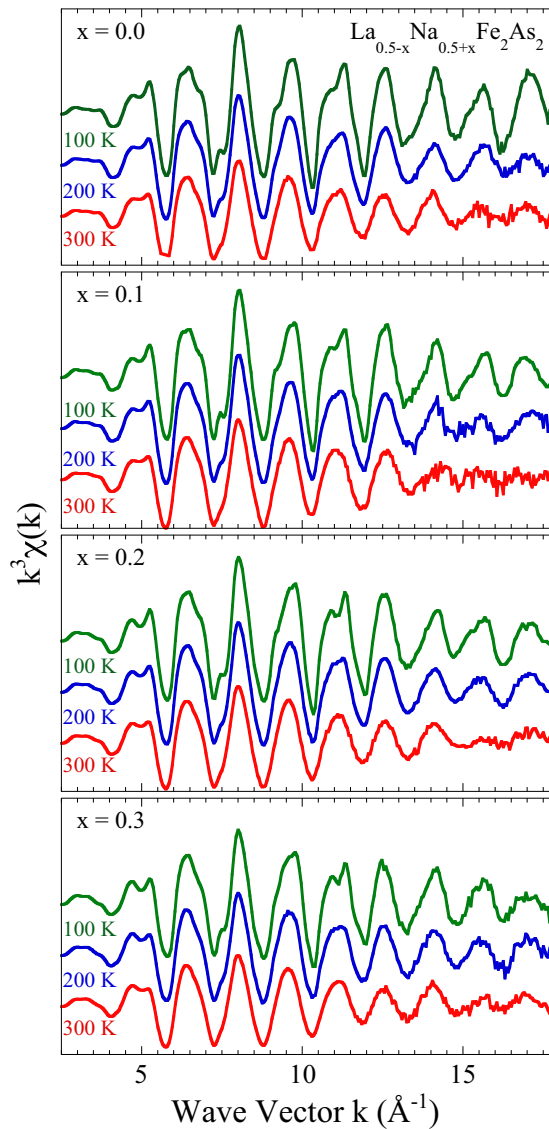


FIG. 1. As K -edge extended x-ray absorption fine structure (EXAFS) oscillations (weighted by k^3) for selected samples of $\text{La}_{0.5-x}\text{Na}_{0.5+x}\text{Fe}_2\text{As}_2$ ($x = 0.0, 0.1, 0.2,$ and 0.3) at representative temperatures.

FT peaks with increasing doping. For example, the main peak in the FT magnitude, representing the As-Fe shell, is much weaker for the doped samples. Incidentally, the FT magnitude hardly shows any appreciable signal beyond 4 \AA ; that is an indication of large overall local configurational disorder in $\text{La}_{0.5-x}\text{Na}_{0.5+x}\text{Fe}_2\text{As}_2$.

The local structural parameters are quantified by EXAFS model fits, for which the conventional approach based on single-scattering approximation [34,35] has been used. The structural parameters obtained by diffraction [8] were used as the starting input parameters for the non-linear least-square fits carried out using the standard EXAFS equation [34,35]:

$$\chi(k) = \sum_i \frac{N_i S_0^2}{k R_i^2} f_i(k, R_i) \exp\left(-\frac{2R_i}{\lambda}\right) \exp(-2k^2 \sigma_i^2) \times \sin[2kR_i + \delta_i(k)],$$

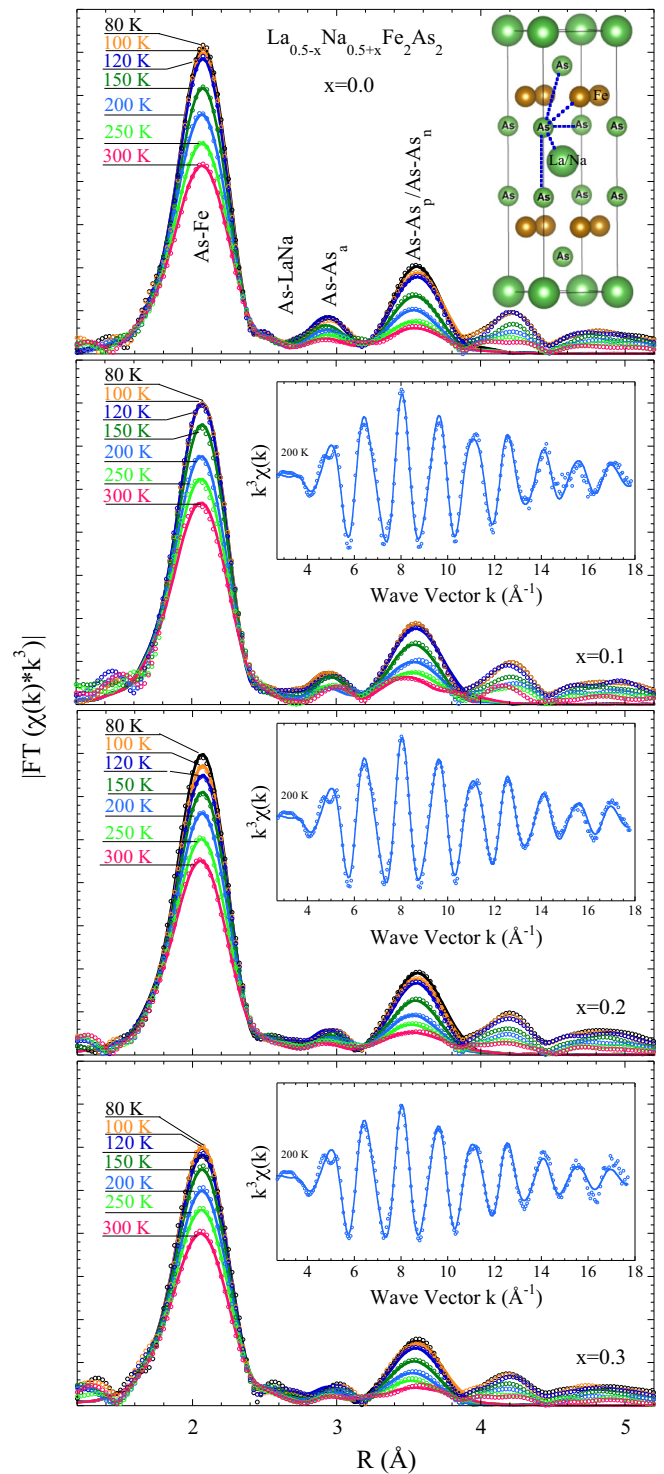


FIG. 2. Fourier transform (FT) magnitudes of As K -edge extended x-ray absorption fine structure (EXAFS) oscillations (weighted by k^3) for selected samples of $\text{La}_{0.5-x}\text{Na}_{0.5+x}\text{Fe}_2\text{As}_2$. The FTs, performed using a Gaussian window in the k range of 2.5 – 17.5 \AA^{-1} , are shown as a function of temperature. The model fits to the FTs are also shown by solid lines. The crystal structure is shown in the upper panel with the near neighbor distances indicated. EXAFS oscillations with model fits are shown for a representative temperature as insets.

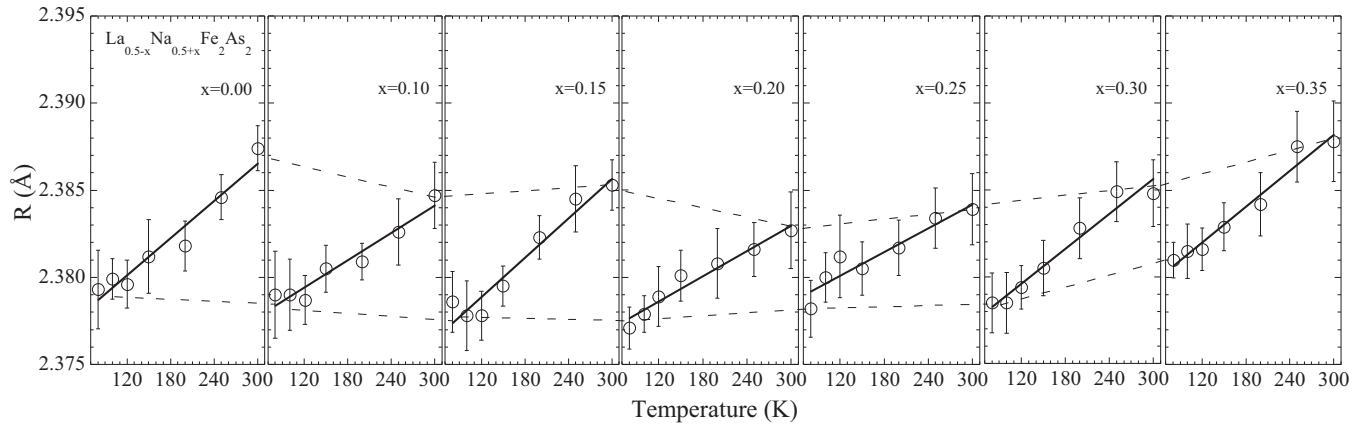


FIG. 3. As-Fe bond lengths in $\text{La}_{0.5-x}\text{Na}_{0.5+x}\text{Fe}_2\text{As}_2$, obtained by extended x-ray absorption fine structure (EXAFS) analysis, are shown as a function of temperature for nominal values of doping. The error bars represent maximum standard deviation, estimated by analyzing different EXAFS scans for any given temperature on each sample. The solid lines are the linear interpolations, while the dashed lines are to guide the changes as a function of doping.

where R_i is the distance between the absorber and scatterer atoms, N_i is the number of near neighbors at distance R_i from the absorber, λ is the mean free path of the photoelectron, $f_i(k, R_i)$ is the scattering amplitude, and δ_i is the phase shift. Here, S_0^2 is the EXAFS reduction factor due to many-body effects, and σ_i^2 describes the mean-square relative displacements (MSRDs) of the absorber-scatterer pair. The model contains five shells including nearest neighbor Fe atoms (i.e., As-Fe distance ~ 2.38 Å), second nearest neighbor La atoms (i.e., As-La distance ~ 3.05 Å), one axial As atom (i.e., As- As_a distance ~ 3.10 Å), four As atoms within the As-As layer (i.e., As- As_p distance ~ 3.84 Å), and four As atoms located in the next layer (i.e., As- As_n distance ~ 3.95 Å). For simplicity, the contribution of Na has been ignored, as this is expected to be small with respect to the scattering factor of La. The scattering amplitudes and phase shifts were calculated using FEFF code [36], while the WINXAS package [37] was used for the model fits. The same results were obtained using the EXCURVE 9.275 code (with calculated backscattering amplitudes and phase shift functions) [38]. The radial distances R_i and the corresponding σ_i^2 were treated as fit parameters, while the coordination numbers were fixed to the nominal values. The S_0^2 was fixed to 0.9, while the energy threshold (E_0) was fixed after fits on reference scans and optimized for each sample. The k range used for the five shells fits was $2.5\text{--}17.5$ Å $^{-1}$, while the R range was $1.4\text{--}4$ Å; therefore, the number of independent data points $N_{\text{ind}} \sim (2\Delta k \Delta R)/\pi$ [34,35] was ~ 25 ($\Delta k = 15$ Å $^{-1}$, and $\Delta R = 2.6$ Å), greater than the fit parameters (10) used in the model. Figure 2 includes the five shell model fits in the real space (solid line). The insets of Fig. 2 (lower, lower middle, and upper middle panels) display k -space EXAFS fit at a representative temperature ($T = 200$ K).

The temperature dependence of the arsenic nearest neighbor As-Fe distance is shown in Fig. 3. The room-temperature values of the As-Fe distance is ~ 2.385 Å, consistent with the mean distance measured by diffraction [8,9]. The As-Fe bond tends to thermally shrink for all dopings with decreasing temperature. The linear thermal expansion coefficient of this bond is $\sim 1 - 2 \times 10^{-5}$ K $^{-1}$, showing a small but evident

variation with doping. The distance hardly shows any doping dependence for $x \leq 0.25$ at low temperature and tends to increase beyond this, while at room temperature, it appears to be almost constant. Thus, the overall shrinkage is smaller for the samples showing optimum transition temperature for $x \geq 0.25$; that is apparent from Fig. 3.

One of the key parameters in the 122 structure is the axial As- As_a bond, regarded as an order parameter for the CT phase transition [8,13]. It has been reported that an As- As_a bond length shorter than ~ 3.15 Å represents a CT phase in LaFe_2As_2 , while it is a UT phase beyond this [13]. Although, the CT phase of CaFe_2As_2 has been found to show much shorter As- As_a bond length, the boundary between the CT to the UT is expected to be ~ 3.11 Å [14,15,17–19]. The information on the As- As_a bond is readily available in the As K -edge EXAFS, and we have determined the same as a function of temperature. We show the temperature dependence of the As- As_a bond length for different samples in Fig. 4(a). The As- As_a bond appears significantly affected by doping and temperature; however, it remains in the range of $\sim 3.06\text{--}3.12$ Å, confirming that all the samples studied here are in their CT phase. This bond length tends to decrease with doping and shows a negative local linear expansion of $\sim -2 \times 10^{-4}$ K $^{-1}$. The linear expansion of this bond is significantly different for the sample with $x = 0.35$, being $\sim -3.5 \times 10^{-4}$ K $^{-1}$. It is possible that small impurity contents are responsible for this deviation since this sample lies near the solubility limit [8]. Nevertheless, the axial As- As_a bond length (at room temperature) tends to contract with doping, and hence, the local magnetic moment is expected to be lower [20] for the optimally doped system. This appears consistent with spin fluctuations reported in nuclear spin relaxation measurements on the optimally doped system [12]. Here, we should mention that the As-La distance hardly shows any temperature dependence and is found to be ~ 3.05 Å (not shown).

The temperature dependence of the local As- As_p bond (representing the in-plane lattice parameter) is shown in Fig. 4(b). The As- As_p bond length also tends to decrease with doping and has a tendency of negative linear thermal expansion for the samples in the optimally doped region.

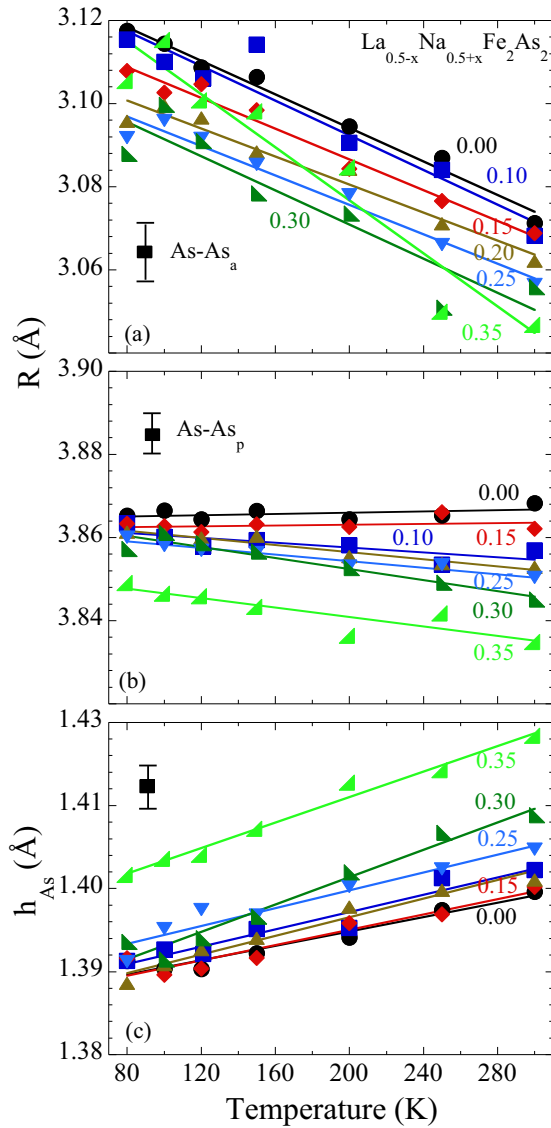


FIG. 4. (a) Axial As-As_a bond lengths and (b) in-plane As-As_p bond lengths (in-plane lattice parameter) in La_{0.5-x}Na_{0.5+x}Fe₂As₂ are shown as a function of temperature. The temperature dependence of the anion height (h_{As}), determined by the As-Fe and in-plane As-As_p bond lengths, is shown for different samples in panel (c). The solid lines are linear interpolation of the temperature dependence. For a clear view of the temperature dependence, error bars are not shown for each data point; instead, maximum uncertainty bars are included in each panel.

Indeed, while linear expansion of this bond for the undoped sample is $\sim 7 \times 10^{-6} \text{ K}^{-1}$, it is in the range of ~ -3 to $-7 \times 10^{-4} \text{ K}^{-1}$ for the optimally doped samples. The anion height (and As-Fe-As bond angle) is an important local structure parameter in the iron-based superconductors, and the T_c is known to be empirically related to it [25]. We can evaluate the anion (As) height with respect to the Fe-Fe plane (h_{As} ; and the As-Fe-As angle) using the trigonometric relationship for the tetragonal lattice with As-Fe and As-As_p bond lengths being the inputs. The As-Fe-As bond angle is in the range of 107 – 109° , suggesting almost perfect tetrahedral FeAs₄ arrangement in La_{0.5-x}Na_{0.5+x}Fe₂As₂. The h_{As} as a function of

temperature for different samples is shown in Fig. 4(c). As expected from the temperature dependence of the input parameters, the h_{As} shows a significant change with temperature. The h_{As} appears to have larger temperature dependence for the optimally doped system than the undoped samples.

In addition to bond lengths, EXAFS provides information on the local vibrational properties through the MSDR parameter (σ_i^2) of near neighbors. Temperature-dependent measurements permit us to obtain information on the correlated atomic displacements characterizing the intrinsic nature of interatomic bonds. The σ_i^2 is a sum of the temperature-independent term σ_0^2 , describing the configurational disorder and the temperature-dependent contribution $\sigma^2(T)$, related with the bonding characteristics, i.e., $\sigma_i^2(T) = \sigma_0^2 + \sigma^2(T)$. Generally, the Einstein model describes satisfactorily the temperature dependence of σ_i^2 for short bonds in which the anharmonic effects are negligible. The model equation to describe the temperature dependence of σ_i^2 can be written as [39,40]

$$\sigma^2(T) = \sigma_0^2 + \frac{\hbar^2}{2k_B\mu\theta_E} \coth\left(\frac{\theta_E}{2T}\right),$$

with μ being the reduced mass of the atoms involved in the bonding and k_B the Boltzmann constant. The θ_E is the Einstein temperature, i.e., the Einstein frequency of the atomic pairs ($\omega_E = k_B\theta_E/\hbar$), that can be used to determine the effective bond stretching force constant through $\kappa = \mu\omega_E^2$. We show σ_i^2 of Fe-As, As-As_a, and As-As_p bond lengths in Fig. 5 as a function of temperature for the different samples. For consistency, the Einstein model fits have been used for all the bonds with θ_E and σ_0^2 being the fit parameters. These fits appear as solid lines in Fig. 5.

The As-Fe bond is well described by the Einstein model with the $\theta_E \sim 307 \text{ K}$ for the undoped sample ($x = 0.0$) that suffers a substantial change with the maximum being for the optimally doped samples (for $x = 0.25$ – 0.35). The σ_0^2 , describing the static disorder, is small ($\sigma_0^2 = 0.0005 \text{ \AA}^2$) for $x = 0.0$; that changes with doping up to $\sim 0.0019 \text{ \AA}^2$ for $x = 0.35$, indicating increased configurational disorder in the As-Fe displacements. These values of θ_E are like the ones found in other pnictides for the As-Fe bonds [27,41–48]. The As-Fe bond stretching is likely to be associated with the infrared active stretching mode (of E_u symmetry); that has been observed at $\sim 250 \text{ cm}^{-1}$ in the optical studies of iron-based superconductors [49–51]. We can determine the effective bond-stretching force constant κ , i.e., the bond stiffness as a function of doping. The $\kappa_{\text{As-Fe}}$ is $\sim 5.3 \text{ eV/\AA}^2$ for the As-Fe bonds in $x = 0.0$; that evolves up to $\sim 6.8 \text{ eV/\AA}^2$ with doping. Since this mode is argued to be one of the important ones for the superconductivity in the iron pnictides, the observation of the hardening with hole doping is interesting due to its direct implication on the Fe $3d$ -As $4p$ orbital overlap and hence the electronic transport properties.

It is apparent from Fig. 5 that axial As-As_a and in-plane As-As_p bonds are substantially weaker than the As-Fe bond. Incidentally, the temperature-dependent σ_i^2 of As-As_a and As-As_p bonds are characterized by similar $\theta_E \sim 214 \text{ K}$ for $x = 0.0$. Unlike the As-Fe bond, the axial As-As_a bond reveals a substantial softening when doped, with the θ_E reducing to

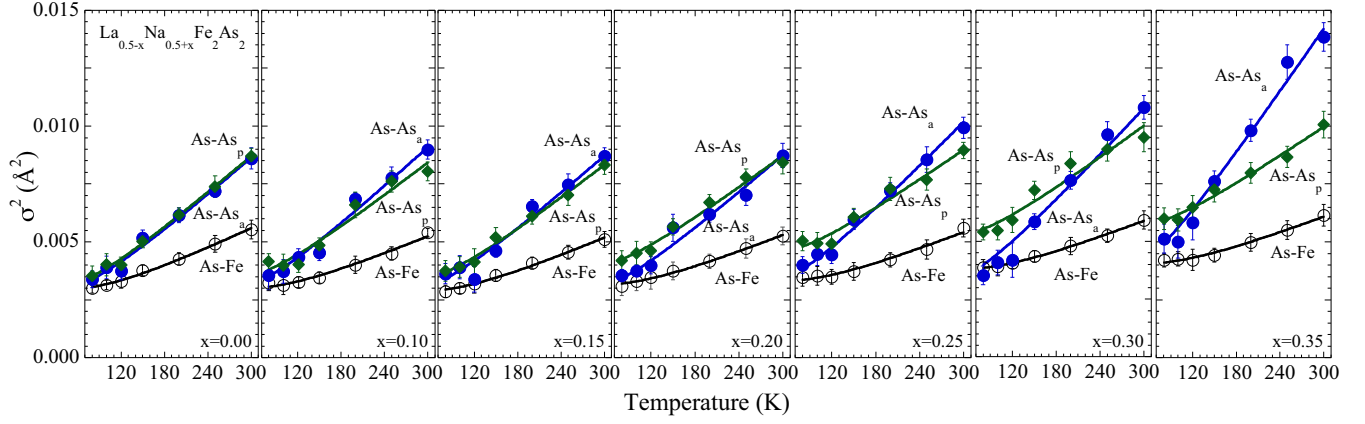


FIG. 5. Mean-square relative displacements (σ^2) of the As-Fe (circles), As-As_a (filled circles), and As-As_p (filled diamonds) bonds in $\text{La}_{0.5-x}\text{Na}_{0.5+x}\text{Fe}_2\text{As}_2$ as a function of temperature for different doping. The solid lines are the Einstein model fits (see text).

~ 166 K for $x = 0.35$. The As-As_p bond suffers a gradual hardening with doping as the case of the As-Fe bond. Indeed, the θ_E of this bond is ~ 214 K for the undoped sample ($x = 0.0$); that increases up to ~ 241 K for $x = 0.35$. Again, the σ_0^2 increases with doping, a mere indication of the increase in an overall configurational disorder due to substitution. We have summarized these local structure parameters in Table I.

Let us discuss the doping dependence of the θ_E . Figure 6 shows the doping dependence of θ_E for the three bonds together with the doping dependence of the As height (at room temperature) and the T_c [Figs. 6(a) and 6(b)]. As discussed above, the θ_E of the As-Fe bond [Fig. 6(c)] increases gradually with doping; however, it tends to saturate for the optimally doped samples ($x = 0.25$ – 0.35), where the superconducting transition temperature [Fig. 6(b)] remains almost doping independent [8,9]. On the other hand, the θ_E of the axial As-As_a bond [Fig. 6(d)] appears to show an opposite trend, i.e., the θ_E of this bond is hardly changing with doping in the interval of underdoping but shows a significant decrease in the optimally doped regime. The large decrease in the θ_E of the axial As-As_a bond suggests that this bond is softer in the optimally doped regime. Instead, the θ_E of the in-plane As-As_p bond [Fig. 6(d)] shows a gradual increase, indicating increased in-plane atomic correlations in the optimally doped regime. The above observations should have some direct effect on the As

height. The doping dependence of the As height is plotted as a function of doping (at room temperature) in Fig. 6(a), showing a gradual increase with doping. Therefore, while the θ_E of the axial As-As_a bond shows a gradual decrease with doping (i.e., the bond is more flexible for the superconducting samples), the As height tends to increase. The fact that the As-As_a distance gets softer in the optimally doped regime and As height gets elongated would suggest that axial motion of As atoms has some important role in the superconductivity of these materials; that should be explored further in detail by theoretical calculations.

Coming back to the axial As-As_a bond length that shows a contraction with doping, this appears to contradict the softening since the shorter axial As-As_a bond is expected to be stronger in the CT phase due to increased dimerization. Therefore, the flexibility of this bond in the superconducting samples could be related with the hardening of the As-Fe bond, i.e., stronger overlap of Fe 3d and As 4p orbitals, while any possible As-As_a dimerization may have limited effect. This is consistent with the theoretical calculations indicating axial As-As_a bonding to be highly sensitive to the As-Fe bond, the Fe 3d-As 4p orbital overlap [17,19], and the suppressed antiferromagnetic order. Although the mean axial As-As_a bond gets shorter with doping, it is more flexible, a mere indication of the role of the axial motion of the As atom in these

TABLE I. The local structure parameters of $\text{La}_{0.5-x}\text{Na}_{0.5+x}\text{Fe}_2\text{As}_2$ determined from As *K*-edge EXAFS. The distances (R_i), with the maximum error of ± 0.003 Å, are provided at room temperature (300 K), while the Einstein temperatures (θ_E) are determined by the temperature dependence of σ_i^2 , i.e., also related with the stretching bond stiffness κ (see text). The temperature-independent terms (σ_0^2) are also included in the table.

$\text{La}_{0.5-x}\text{Na}_{0.5+x}\text{Fe}_2\text{As}_2$	As-Fe			As-As _a			As-As _p		
	θ_E (Å)	κ (eV/Å ²)	σ_0^2 (Å ²)	θ_E (Å)	κ (eV/Å ²)	σ_0^2 (Å ²)	θ_E (Å)	κ (eV/Å ²)	σ_0^2 (Å ²)
0.00	307 ± 8	5.3 ± 0.1	0.0005(2)	214 ± 6	3.0 ± 0.1	0.0001(1)	214 ± 8	3.0 ± 0.1	0.0002(2)
0.10	321 ± 7	5.8 ± 0.1	0.0006(3)	207 ± 6	2.9 ± 0.1	0.0001(1)	227 ± 8	3.4 ± 0.1	0.0007(4)
0.15	324 ± 9	6.0 ± 0.2	0.0006(3)	212 ± 6	3.0 ± 0.1	0.0001(1)	226 ± 9	3.4 ± 0.1	0.0006(4)
0.20	334 ± 9	6.3 ± 0.2	0.0009(3)	213 ± 6	3.0 ± 0.1	0.0001(1)	228 ± 9	3.4 ± 0.1	0.0011(4)
0.25	336 ± 8	6.4 ± 0.2	0.0011(4)	196 ± 6	2.6 ± 0.1	0.0001(1)	237 ± 10	3.7 ± 0.2	0.0019(4)
0.30	339 ± 9	6.5 ± 0.2	0.0016(3)	191 ± 8	2.4 ± 0.1	0.0001(1)	225 ± 10	3.4 ± 0.2	0.0024(4)
0.35	345 ± 9	6.8 ± 0.2	0.0019(4)	166 ± 4	1.8 ± 0.1	0.0001(1)	241 ± 12	3.9 ± 0.2	0.0030(5)

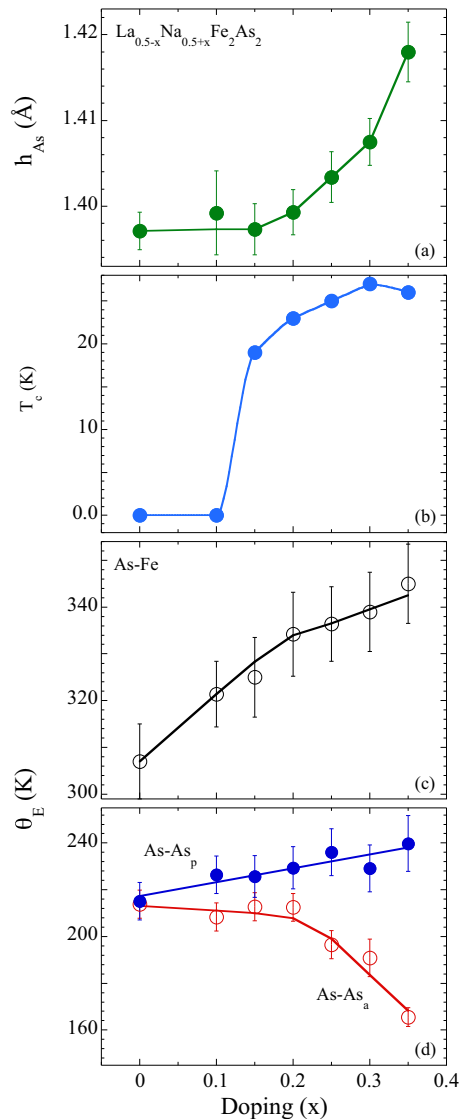


FIG. 6. (a) The doping-dependent anion height (h_{As} in $\text{La}_{0.5-x}\text{Na}_{0.5+x}\text{Fe}_2\text{As}_2$ at room temperature. (b) The T_c vs doping phase diagram [8]. (c) The Einstein temperature (θ_E) of the As-Fe bond. (d) The θ_E of axial As-As_a and in-plane As-As_p bonds as a function of doping.

materials. This would be consistent with the increased anion height in the optimally doped regime, as shown in Fig. 6(a). This agrees well with the *ab initio* calculations showing the optimized As height to increase continuously with hole doping [52], however remaining constant in the electron doped regime.

The As-Fe bond gets stronger with doping, and hence, a stronger As 4*p*-Fe 3*d* orbital hybridization is expected. This information is available in the x-ray absorption near edge structure (XANES) region of the As *K*-edge absorption spectra. Indeed, XANES probes higher order atomic correlation function; thus, it is highly sensitive to the local geometry and the valence electronic states [34,35]. We have plotted the As *K*-edge XANES spectra of $\text{La}_{0.5-x}\text{Na}_{0.5+x}\text{Fe}_2\text{As}_2$ at room temperature in Fig. 7 for all the samples. The spectra are normalized with respect to the atomic absorption estimated from

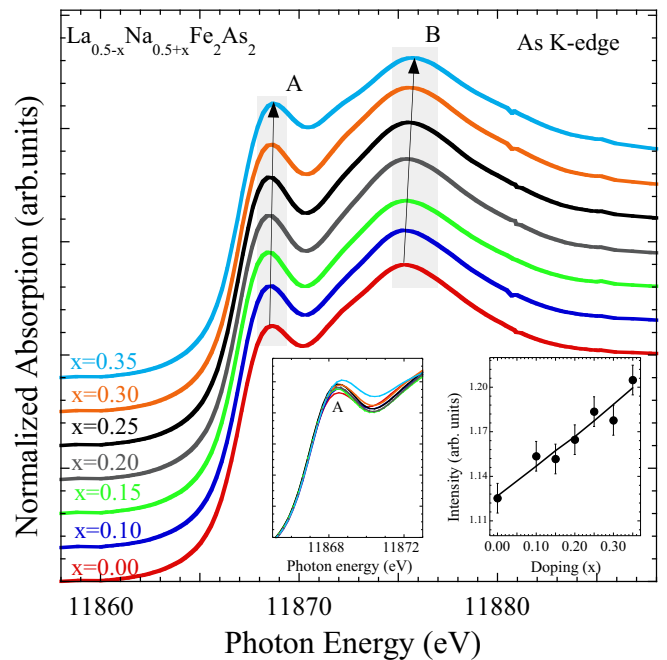


FIG. 7. Normalized As *K*-edge x-ray absorption near edge structure (XANES) spectra of $\text{La}_{0.5-x}\text{Na}_{0.5+x}\text{Fe}_2\text{As}_2$ at room temperature. There are two main features denoted by A and B. The left inset shows a zoom over the main peak feature A. The right inset shows the intensity of feature A as a function of doping. The error bars in the intensity represent maximum error estimated by analyzing four different scans for each sample.

the high-energy part of the absorption spectra. The XANES spectra are characterized by two main spectral features, a peak feature A and a broad feature B. The peak feature A, well separated from the broad structure B, is related to the dipole allowed transition from the As 1*s* level to the unoccupied As 4*p* admixed with the Fe 3*d* states, while the structure B is a multiple-scattering feature involving admixed states from different near neighbor orbitals [53–55] and hence a sensitive probe of the local geometry. The feature B reveals a shift toward higher energy; that is consistent with a decreased in-plane lattice parameter in the system as a function of doping [8]. Both features show changes in the spectral intensity with doping; however, the change in the peak feature A intensity is substantial (see, e.g., a zoom over the peak A in the left inset). The peak feature A provides a direct measure of the unoccupied electronic states and hence a measure of the overlap between As 4*p* and Fe 3*d* orbitals in the valence band. We have plotted the spectral intensity of the peak feature A as a function of doping in the inset (right) of Fig. 7. The peak feature A shows a gradual increase in the spectral intensity as a function of doping, with a maximum change being $\sim 8\%$ of the normalized absorption. Being a probe of As 4*p* states, this behavior suggests that the electronic structure of 4*p* states changes with the hardening of the As-Fe bond [Fig. 6(c)]. The stronger (weaker) overlap corresponds to a stronger (weaker) As-Fe bond and hence higher (lower) spectral intensity of the feature A in the As *K*-edge XANES. Therefore, the changes in the XANES features are consistent with the local structure of the As-Fe bond stiffness in $\text{La}_{0.5-x}\text{Na}_{0.5+x}\text{Fe}_2\text{As}_2$.

Finally, it is interesting to note the analogy between different families of superconductors showing importance of the axial atomic correlations. For example, in copper oxide superconductors, the axial Cu-O bond has a direct correlation with the superconducting transition temperature [56]. Indeed, it has been found that the axial Cu-O distance controls the formation of an admixed state involving Cu $4s$, Cu $3d_{3z^2-r^2}$, and axial oxygen $2p_z$ orbitals; that induces charge localization/delocalization [57]. Incidentally, BiS₂-based superconductors also show a direct correlation between T_c and the axial Bi-S distance, where the axial Bi-S distance controls the admixing of Bi $6s$, Bi $6p_z$, and axial S $3p_z$ orbitals and hence the charge transfer [58]. Therefore, axial As atom correlations reflected through As height and hence the As $4p_z$ orbitals in the iron-based superconductors appear to have a similar role as axial oxygen in cuprates and axial sulfur in BiS₂-based superconductors.

IV. CONCLUSIONS

In summary, the local structure of the La_{0.5-x}Na_{0.5+x}Fe₂As₂ superconductor has been studied

as a function of temperature and doping. The measurements reveal a substantial change in the local structure with the near neighbor bonds evolving systematically with the hole doping and temperature. The axial As-As_a bond length indicates the system to be in the CT phase. The As-Fe bond is relatively weak in the undoped samples; that gets stronger with doping. The axial As-As_a bond is found to get weaker in the optimally doped regime. The arsenic height shows an increase in the optimally doped superconducting phase, while it remains almost constant in undoped or underdoped samples. The results suggest the vital role of axial As atom fluctuations in the superconductivity of these iron-based materials. Such fluctuations are expected to be important in the context of the short-range nematicity and mesoscopic order in the iron-based superconductors.

ACKNOWLEDGMENTS

The authors thank the ALBA CLAESS beamline staff for support during the experimental run. This paper is partially supported by the Sapienza University of Rome and JSPS Kakenhi (Grants No. JP19H05823 and No. JP19H00659).

-
- [1] Y. Kamihara, T. Watanabe, M. Hirano, and H. Hosono, *J. Am. Chem. Soc.* **130**, 3296 (2008).
- [2] H. Hosono and K. Kuroki, *Physica C* **514**, 399 (2015).
- [3] G. R. Stewart, *Rev. Mod. Phys.* **83**, 1589 (2011).
- [4] H. Hosono, A. Yamamoto, H. Hiramatsu, and Y. Ma, *Mater. Today* **21**, 278 (2018).
- [5] A. Iyo, K. Kawashima, T. Kinjo, T. Nishio, S. Ishida, H. Fujihisa, Y. Gotoh, K. Kihou, H. Eisaki, and Y. Yoshida, *J. Am. Chem. Soc.* **138**, 3410 (2016).
- [6] K. Kawashima, S. Ishida, H. Fujihisa, Y. Gotoh, K. Kihou, Y. Yoshida, H. Eisaki, H. Ogino, and A. Iyo, *J. Phys. Chem. Lett.* **9**, 868 (2018).
- [7] B. Q. Song, Manh Cuong Nguyen, C. Z. Wang, and K. M. Ho, *Phys. Rev. B* **97**, 094105 (2018).
- [8] A. Iyo, K. Kawashima, S. Ishida, H. Fujihisa, Y. Gotoh, H. Eisaki, and Y. Yoshida, *J. Am. Chem. Soc.* **140**, 369 (2018).
- [9] A. Iyo, K. Kawashima, S. Ishida, H. Fujihisa, Y. Gotoh, Y. Yoshida, and H. Eisaki, *Inorg. Chem.* **57**, 9223 (2018).
- [10] Y. Gu, J.-O. Wang, X. Ma, H. Luo, Y. Shi, and S. Li, *Supercond. Sci. Technol.* **31**, 125008 (2018).
- [11] J.-Q. Yan, S. Nandi, B. Saparov, P. Čermák, Y. Xiao, Y. Su, W. T. Jin, A. Schneidewind, T. Brückel, R. W. McCallum, T. A. Lograsso, B. C. Sales, and D. G. Mandrus, *Phys. Rev. B* **91**, 024501 (2015).
- [12] T. Kouchi, M. Yashima, H. Mukuda, S. Ishida, H. Eisaki, Y. Yoshida, K. Kawashima, and A. Iyo, *J. Phys. Soc. Jpn.* **88**, 113702 (2019).
- [13] A. Iyo, S. Ishida, H. Fujihisa, Y. Gotoh, I. Hase, Y. Yoshida, H. Eisaki, and K. Kawashima, *J. Phys. Chem. Lett.* **10**, 1018 (2019).
- [14] A. Kreyssig, M. A. Green, Y. Lee, G. D. Samolyuk, P. Zajdel, J. W. Lynn, S. L. Bud'ko, M. S. Torikachvili, N. Ni, S. Nandi, J. B. Leão, S. J. Poulton, D. N. Argyriou, B. N. Harmon, R. J. McQueeney, P. C. Canfield, and A. I. Goldman, *Phys. Rev. B* **78**, 184517 (2008).
- [15] A. I. Goldman, A. Kreyssig, K. Prokeš, D. K. Pratt, D. N. Argyriou, J. W. Lynn, S. Nandi, S. A. J. Kimber, Y. Chen, Y. B. Lee, G. Samolyuk, J. B. Leão, S. J. Poulton, S. L. Bud'ko, N. Ni, P. C. Canfield, B. N. Harmon, and R. J. McQueeney, *Phys. Rev. B* **79**, 024513 (2009).
- [16] F. Wei, B. Lv, L. Deng, J. K. Meen, Y.-Y. Xue, and C.-W. Chu, *Philos. Mag.* **94**, 2562 (2014).
- [17] T. Yildirim, *Phys. Rev. Lett.* **102**, 037003 (2009).
- [18] R. Yang, C. Le, L. Zhang, B. Xu, W. Zhang, K. Nadeem, H. Xiao, J. Hu, and X. Qiu, *Phys. Rev. B* **91**, 224507 (2015).
- [19] J. Diehl, S. Backes, D. Guterding, H. O. Jeschke, and R. Valenti, *Phys. Rev. B* **90**, 085110 (2014).
- [20] K. Zhao, J. K. Glasbrenner, H. Gretarsson, D. Schmitz, J. Bednarcik, M. Etter, J. P. Sun, R. S. Manna, A. Al-Zein, S. Lafuerza, W. Scherer, J. G. Cheng, and P. Gegenwart, *Phys. Rev. B* **97**, 020510(R) (2018).
- [21] I. I. Mazin, M. Shimizu, N. Takemori, and H. O. Jeschke, *Phys. Rev. Lett.* **123**, 267001 (2019).
- [22] H. Usui and K. Kuroki, *Phys. Rev. Research* **1**, 033025 (2019).
- [23] X. Luo and X. Chen, *Sci. China Mater.* **58**, 77 (2015).
- [24] D. Johrendt, *J. Mater. Chem.* **21**, 13726 (2011).
- [25] Y. Mizuguchi, Y. Hara, K. Deguchi, S. Tsuda, T. Yamaguchi, K. Takeda, H. Kotegawa, H. Tou, and Y. Takano, *Supercond. Sci. Technol.* **23**, 054013 (2010).
- [26] C. Cantoni, M. A. McGuire, B. Saparov, A. F. May, T. Keiber, F. Bridges, A. S. Sefat, and B. C. Sales, *Adv. Mater.* **27**, 2715 (2015).
- [27] F. Stramaglia, G. M. Pugliese, L. Tortora, L. Simonelli, C. Marini, W. Olszewski, S. Ishida, A. Iyo, H. Eisaki, T. Mizokawa, and N. L. Saini, *J. Phys. Chem. C* **125**, 10810 (2021).

- [28] J.-H. Kang, J.-W. Kim, P. J. Ryan, L. Xie, L. Guo, C. Sundahl, J. Schad, N. Campbell, Y. G. Collantes, E. E. Hellstrom, M. S. Rzchowski, and C.-B. Eom, *Proc. Natl. Acad. Sci. USA* **117**, 21170 (2020).
- [29] J. Wang, Y. Wu, X. Zhou, Y. Li, B. Teng, P. Dong, J. He, Y. Zhang, Y. Ding, and J. Li, *Adv. Phys.: X* **6**, 1878931 (2021).
- [30] S. Wu, Y. Song, Y. He, A. Frano, M. Yi, X. Chen, H. Uchiyama, A. Alatas, A. H. Said, L. Wang, T. Wolf, C. Meingast, and R. J. Birgeneau, *Phys. Rev. Lett.* **126**, 107001 (2021).
- [31] B. A. Frandsen, K. M. Taddei, D. E. Bugaris, R. Stadel, M. Yi, A. Acharya, R. Osborn, S. Rosenkranz, O. Chmaissem, and R. J. Birgeneau, *Phys. Rev. B* **98**, 180505(R) (2018).
- [32] T. Shimojima, Y. Motoyui, T. Taniuchi, C. Bareille, S. Onari, H. Kontani, M. Nakajima, S. Kasahara, T. Shibauchi, Y. Matsuda, and S. Shin, *Science* **373**, 1122 (2021).
- [33] L. Simonelli, C. Marini, W. Olszewski, M. Ávila Pérez, N. Ramanan, G. Guilera, V. Cuartero, and K. Klementiev, *Cogent Phys.* **3**, 1231987 (2016).
- [34] D. C. Koningsberger and R. Prins, *X-Ray Absorption: Principles, Applications, Techniques of EXAFS, SEXAFS and XANES* (Wiley, Chichester, 1988).
- [35] G. Bunker, *Introduction to XAFS* (Cambridge University Press, Cambridge, 2010).
- [36] A. L. Ankudinov, B. Ravel, J. J. Rehr, and S. D. Conradson, *Phys. Rev. B* **58**, 7565 (1998).
- [37] T. Ressler, *J. Synchrotron Radiat.* **5**, 118 (1998).
- [38] S. J. Gurman, *J. Synchrotron Radiat.* **2**, 56 (1995).
- [39] E. Sevillano, H. Meuth, and J. J. Rehr, *Phys. Rev. B: Condens. Matter Mater. Phys.* **20**, 4908 (1979).
- [40] See, e.g., a review by J. J. Rehr and R. C. Albers, *Rev. Mod. Phys.* **72**, 621 (2000).
- [41] T. A. Tyson, T. Wu, J. C. Woicik, B. Ravel, A. Ignatov, C. L. Zhang, Z. Qin, T. Zhou, and S.-W. Cheong, *J. Appl. Phys.* **108**, 123715 (2010).
- [42] W. Chu, J. Cheng, S. Chu, T. Hu, and A. Marcelli, X. Chen, and Z. Wu, *Sci. Rep.* **3**, 1750 (2013).
- [43] B. Joseph, A. Iadecola, L. Malavasi, and N. L. Saini, *J. Phys.: Condens. Matter* **23**, 265701 (2011).
- [44] B. Joseph, A. Iadecola, L. Simonelli, L. Maugeri, A. Martinelli, A. Palenzona, M. Putti, and N. L. Saini, *Supercond. Sci. Technol.* **26**, 065005 (2013).
- [45] M. Y. Hacisalihoglu, L. Simonelli, C. Marini, A. Provino, A. Martinelli, P. Manfrinetti, M. Putti, and N. L. Saini, *J. Phys.: Condens. Matter* **33**, 095803 (2021).
- [46] E. Paris, B. Joseph, A. Iadecola, C. Marini, K. Kudo, D. Mitsuoka, M. Nohara, T. Mizokawa, and N. L. Saini, *Phys. Rev. B* **90**, 094508 (2014).
- [47] E. Paris, T. Wakita, O. Proux, T. Yokoya, K. Kudo, D. Mitsuoka, T. Kimura, K. Fujimura, N. Nishimoto, S. Ioka, M. Nohara, T. Mizokawa, and N. L. Saini, *Phys. Rev. B* **96**, 224507 (2017).
- [48] E. Paris, T. Wakita, L. Simonelli, C. Marini, W. Olszewski, K. Terashima, F. Stramaglia, G. M. Pugliese, T. Mizokawa, S. Ioka, K. Kudo, M. Nohara, T. Yokoya, and N. L. Saini, *Supercond. Sci. Technol.* **32**, 095001 (2019).
- [49] Z. G. Chen, R. H. Yuan, T. Dong, and N. L. Wang, *Phys. Rev. B* **81**, 100502(R) (2010).
- [50] B. Xu, E. Cappelluti, L. Benfatto, B. P. P. Mallett, P. Marsik, E. Sheveleva, F. Lyzwa, Th. Wolf, R. Yang, X. G. Qiu, Y. M. Dai, H. H. Wen, R. P. S. M. Lobo, and C. Bernhard, *Phys. Rev. Lett.* **122**, 217002 (2019).
- [51] R. Yang, Y. Dai, B. Xu, W. Zhang, Z. Qiu, Q. Sui, C. C. Homes, and X. Qiu, *Phys. Rev. B* **95**, 064506 (2017).
- [52] Y. Yang, S.-Q. Feng, H.-Y. Lu, W.-S. Wang, and Z.-P. Chen, *J. Super. Novel Mag.* **32**, 855 (2019).
- [53] W. Xu, B. Joseph, A. Iadecola, A. Marcelli, W. Chu, D. Di Gioacchino, A. Bianconi, Z. Wu, and N. Saini, *Europhys. Lett.* **90**, 57001 (2010).
- [54] B. C. Chang, Y. B. You, T. J. Shiu, M. F. Tai, H. C. Ku, Y. Y. Hsu, L. Y. Jang, J. F. Lee, Z. Wei, K. Q. Ruan, and X. G. Li, *Phys. Rev. B* **80**, 165108 (2009).
- [55] A. Iadecola, B. Joseph, L. Simonelli, L. Maugeri, M. Fratini, A. Martinelli, A. Palenzona, M. Putti, and N. L. Saini, *Phys. Rev. B* **85**, 214530 (2012).
- [56] E. Pavarini, I. Dasgupta, T. Saha-Dasgupta, O. Jepsen, and O. K. Andersen, *Phys. Rev. Lett.* **87**, 047003 (2001).
- [57] Y. Y. Peng, G. Della, M. Minola, M. Conni, A. Amorese, D. Di Castro, G. M. De Luca, K. Kummer, M. Salluzzo, X. Sun, X. J. Zhou, G. Balestrino, M. Le Tacon, B. Keimer, L. Braicovich, N. B. Brookes, and G. Ghiringhelli, *Nat. Phys.* **13**, 1201 (2017).
- [58] G. M. Pugliese, E. Paris, F. G. Capone, F. Stramaglia, T. Wakita, K. Terashima, T. Yokoya, T. Mizokawa, Y. Mizuguchi, and N. L. Saini, *Phys. Chem. Chem. Phys.* **22**, 22217 (2020).